Patient-Derived Microvesicles/AIE Luminogen Hybrid System for Personalized Sonodynamic Cancer Therapy in Patient-Derived Xenograft Models

Daoming Zhu, Zheng Zheng, Meng Suo, Zeming Liu, Yanhong Duo and Ben Zhong Tang**

Dr. D. Zhu, Prof. Y. Duo
Department of Radiation Oncology, the Second Clinical Medical College of Jinan University, 1st Affiliated Hospital of Southern University of Science and Technology, Shenzhen People's Hospital, Shenzhen 518020, China.
E-mail: yanhong.duo@ki.se

Dr. Z. Zheng, Prof. B. Z. Tang
Department of Chemistry, Hong Kong Branch of Chinese National Engineering Research Center for Tissue Restoration and Reconstruction, Institute for Advanced Study and Department of Chemical and Biological Engineering, The Hong Kong University of Science and Technology, Clear Water Bay, Kowloon, Hong Kong, China.
E-mail: tangbenz@ust.hk

Dr. D. Zhu, Dr. M. Suo
Department of Electronic Science and Technology, School of Physics and Technology, Wuhan University, Wuhan 430072, China.

Prof. Z. Liu
Department of Plastic Surgery, Zhongnan Hospital of Wuhan University, Wuhan, 430071, China.
E-mail: 6myt@163.com

D. Z., and Z. Z. contributed equally to this work.

Keywords: Aggregation-Induced Emission, Sonosensitizers, Personalized Sonodynamic Cancer Therapy, Patient-Derived Microvesicles, Patient-Derived Xenograft Models

Abstract

Sonodynamic therapy (SDT), as an efficient way of tumor treatment, has the advantages of deep tumor penetration and high therapeutic efficacy. However, developing efficient sonosensitizers are still challenging. AIEgen-based SDT has never been reported and it is urgent to develop novel AIEgen-active sonosensitizers. Furthermore, the AIEgen-based theranostic system is promisingly needed to be proved on PDX models to be closer to the clinic. Herein, we constructed the first AIEgen based SDT system and found that DCPy has advantages over traditional sonosensitizers in SDT. Then, a patient-derived MVs/AIEgen hybrid system prepared by electroporation was used for personalized SDT in bladder cancer patient-derived xenograft (PDX) models. Impressively, AMVs displayed the superior tumor targeting ability and efficient personalized SDT therapy on PDX models, both of which were much more improved compared with PLGA/AIEgens nanoparticles and cell line-derived micro vesicles. This work presented the first example of an AIEgen-based hybrid system as sonosensitizer for SDT and provides new ideas for both the design of AIE-active sonosensitizers and the SDT treatment of cancers, further expanding the potential clinical

application of AIEgens in the future.

Introduction

Aggregation-induced emission (AIE)-active fluorophores exhibit intense emissions in the aggregated form compared with their monomeric form.[1] The high photostability, biocompatibility, as well as high-contrast imaging of the AIE luminogens (AIEgens) makes them the perfect bioimaging tool.[2] Also, AIEgens find applications in photodynamic therapy (PDT), a non-invasive cancer treatment, since they act as a source of reactive oxygen species (ROS) under light.[3-5, 6] AIEgen-based photosensitizers (PS) have assisted in the development of new PDT strategies.[7] Although the research of AIEgens in photodynamic therapy has been rapidly developed, the inherent defects of PDT still limit the clinical application of AIEgens, including low penetration depth since light is fundamental for the activation of the sensitizers, and the short half-life (<0.04 μs) and high reactivity of ROS, which localizes its impact within 0.02 μm of the point of origin.[8] These limitations restrict the application of PDT to either superficial or endoscopically reachable tumors, such as skin cancer. Also, restricted exposure to sunlight post-PDT presents an added disadvantage to the patients.

Ultrasound (US) waves are high frequency (> 20 kHz) inaudible waves that are widely used in cancer therapeutics as they possess high tissue penetration ability while avoiding radiation damage compared with alternative diagnostic-imaging tools.[9, 10] Sonodynamic therapy (SDT) uses US combined with a sonosensitizer to kills cancer cells by using sonochemistry, sonoporation, and sonoluminescence to activate ROS-producing sonosensitizer molecules, such as hematoporphyrin. [11] In addition, the deep penetration and high therapeutic efficacy of SDT make it a promising cancer therapy. However, the conventional organic sonosensitizing molecules have low bioavailability and are biochemically unstable, resulting in reduced therapeutic efficiency of SDT and its clinical applications.[9, 12] Previous studies have demonstrated the efficiency of inorganic nanoparticles, such as TiO_2 in enhancing the efficacy of SDT.[13] However, the difficulty in biodegradation and uncertain biosafety issues restrict their use.[14] Therefore, it is promising to develop sonosensitizers with good safety and high efficiency. Given AIEgen's many diagnostic and therapeutic advantages, the use of AIEgen in SDT has also attracted our attention, and there have been no research on the AIEgen based SDT.

Furthermore, AIEgen for SDT may be limited by its hydrophobic and poor tumor-targeting ability.[6, 15] Additionally, low target efficiency, low encapsulation efficiency (EE), and poor tissue permeability also limit the practical use of the most previously reported drug delivery systems for AIEgen.[5, 15, 16] Therefore, developing a novel AIEgen-based nanoparticle platform with good targeting efficiency and high EE and tissue permeability for SDT is promising. Recently, the utilization of cell-derived microvesicles (MVs) presents a novel method for drug delivery.[17, 18] MVs are secreted by the cellular membrane in response to an endogenous/exogenous stimulus. MVs are approximately 100–1000 nm in diameter, contain macromolecules, such as proteins, lipids, nucleic acids from the parent cell.[18] Previous studies have demonstrated the efficiency of MVs in cancer treatment.[19, 20] MVs have a high loading capacity for hydrophobic drugs. They undergo cellular absorption and internalization depending on the protein composition in the MVs membrane and cell surface-receptors.[19] Therefore, the idea of developing the MVs/AIEgen hybrid system for SDT is coming out. Currently, the synthesis and evaluation of the MVs have been mostly performed on cell lines and cell-line-derived xenograft (CDX) mouse models.[21, 22] Considering cell lines and human-

derived cells elicit a considerably different response, the translation of this novel MVs/AIEgen hybrid system into clinical applications remains dubious. Moreover, the efficacy evaluation of these proposed MVs/AIEgen in CDX mouse models would lack accuracy because these models would have undergone irreversible physiological changes and would have adapted to the in vitro tumor environment.[23] Additionally, the heterogeneity and complexity of the primary human tumor tissue (extracellular matrix barrier, interstitial pressure, etc.) would impact the mechanism of action of the nanomedicines as well as the tolerability, sensitivity, and distribution of ROS produced during the PDT/SDT process.[24] Compared with CDX model, the patient-derived xenograft (PDX) model would conserve any histological changes and intratumoral heterogeneity from the primary human cancer tissues, along with the regenerative tumor microenvironment (TME), including tumor stroma and blood vessels, supporting the reliability of the PDX model for the preclinical assessments of nanomedicines.[25] So far, there have been no studies on the application of AIEgens or AIEgens-based nanoparticles for the PDT or/and SDT treatment in the PDX model.

Herein, the feasibility of the patient-derived MVs/AIEgen hybrid system in the PDX model for personalized SDT in bladder cancer patient-derived xenograft models was evaluated. Initially, the PDX cell/mouse models were developed by collecting tumor tissues from patients with bladder tumors (Scheme 1). Then, the patient-derived cancer cells (PCCs) were isolated from the tumor tissues of the patients, and they were then prepared into extracellular vesicles (PCVs). Subsequently, the patient-derived MVs/AIEgen hybrid system (AMVs) was prepared using the electroporation method. The experiments in PDX models showed that the AMVs could effectively target the homologous tumor cells/tissues. Also, significant binding was observed if the donor MVs matched the host cells in vitro. Compared with PLGA/AIEgens nanoparticles (APs) and MVs/AIEgens derived from a cell line (ALVs), AMVs had the much improved tumor-targeting ability, suggesting the personalized treatment characteristics of AMVs. Furthermore, we found that AIEgen (named DCPy) used in our experiments can be as an excellent sonosensitizer. Under the irradiation of sound waves, DCPy can simultaneously produce singlet oxygen ($^1O_2$) and hydroxyl radical (•OH) to kill PCCs, and the ROS generation is superior to that of traditional sonosensitizer. This is the first example of AIEgen being used as a sonosensitizer and also the first time that patients-derived vesicles and AIEgen were hybridized for the treatment of the PDX model. This system has demonstrated a good SDT therapeutic effect in the PDX model, which provides new ideas for both SDT treatment and AIEgens designing, and further expands the clinical application of AIEgens in the future.

Results and Discussion

DCPy ((E)-4-(2-(7-(diphenylamino)-9-ethyl-9H-carbazol-2-yl) vinyl)-1-methylpyridin-1-ium hexafluorophosphate) was synthesized (75-80% pure) following a previously described method.[4] NMR and high-resolution mass spectrometry (MS) were used to characterize the intermediates and products (Figure S1-S3). Then, PCVs and microvesicles, which were from T24 cells, were prepared by an ultraviolet stimulation method and exhibited spherical vesicles (Figure 1A). AMVs (~ 300 nm) were prepared through electroporation, which did not change their morphology significantly (Figure 1B and S6). Next, the membrane fluorescent probe 3, 3-Dioctadecyloxacarbocyanine perchlorate (DiO) was used to establish successful DCPy coupling in these AMVs, followed by confocal microscopic analysis, which revealed both red DCPy and bright green DiO fluorescence confirming the coupling reaction (Figure 1C). The stability of AMVs and PCVs was conducted and the insignificant change in their size or zeta

potential after 3-day storage at 4°C in PBS was observed (Figure 1D and S4). Photoluminescence (PL) spectra analysis showed that the DCPy solution (in 100% DMSO) showed poor fluorescence and the AMVs (in PBS) and DCPy (aggregated in a 90% water-DMSO solution) showed the strong emission peaked at 672 nm and 698 nm, respectively (Figure S5). A blue shift of 26 nm in the PL of DCPy suggested the successful synthesis of the AMVs. We also hybridized DCPy with T24 cell-derived extracellular vesicles (ALVs) as a non-homologous control group against PCCs (Figure S7). The FDA-approved poly (lactic-co-glycolic) acid (PLGA) was used to prepare the PLGA/DCPy hybrid nanoparticles (APs) to compare with AMVs in the *in vitro* and *in vivo* experiments.[26] The results of transmission electron microscopy (TEM) revealed that these nanoparticles had a spherical shape and homogenous size (Figure S8). An increase in DCPy electroporation efficiency values was observed by increasing DCPy concentration until it reached a maximum value of 80.6 ± 2.9 % (Figure S9). A characteristic peak of DCPy was observed in the UV-vis absorption spectra for both AMVs and APs, confirming their successful coupling with DCPy (Figure S10).

Next, electron spin resonance (ESR) was used to detect ROS ($^1O_2$ and •OH). We mixed 2, 2, 6, 6-tetramethylpiperide (trapping agent) with PBS, Ce6, and DCPy (each 10 μg/mL), respectively, followed by US irradiation (1.0 MHz, 0.75 W/cm^2, 1 min). DCPy showed an increase in the peak intensity by 2.8% compared with Ce6 (Figure 1E). Thus, DCPy possessed $^1O_2$ generation ability comparable to Ce6 (a conventional sonosensitizers) post-irradiation with US. For detecting •OH, 5, 5-dimethyl-1-pyrroline-N-oxide was used as the trapping agent by keeping other procedures consistent with $^1O_2$ detection. The peak intensity of DCPy increased by 79.0% compared with Ce6 (Figure 1F), indicating that it could generate •OH efficiently post US irradiation. Sodium dodecyl sulfate-polyacrylamide gel electrophoresis (SDS-PAGE) bands demonstrated that AMVs obtained the protein contents from PCVs (Figure 1G). The decomposition of ABDA and methylene blue are consistent with the ESR results (Figure 1H and 1I). Further, AMVs and ALVs exhibited higher $^1O_2$ generation efficiency as compared to APs according to ABDA decomposition experiments (Figure 1J) probably due to the loose packing of AMVs, which resulted in improved oxygen diffusion inside the thin lipid bilayer, compared with the APs where the DCPy formed large solid aggregates, restricting the exposure of deeply embedded PSs to free oxygen. [27] In general, DCPy, as the first AIEgen to be studied for SDT, can efficiently produce $^1O_2$ and •OH under US irradiation, which has a good potential for SDT in clinical and inspires us to proceed to the next biological experiment. It should be noted that according to our previous work, $^1O_2$ production of DCPy under light irradiation is stronger than the Ce6.[4] While our experimental results showed that the DCPy has the same $^1O_2$ production capacity as Ce6 under US. This is interesting and shows that mechanism of DCPy producing $^1O_2$ and •OH probably activated by ultrasonic cavitation effect rather than sonoluminescence.[28]

We have previously demonstrated that post-internalization DCPy specifically targets mitochondria in cancer cells.[4] We performed a colocalization experiment involving the incubation of PCCs with AMVs, DCPy, APs or ALVs, followed by staining with a commercial mitochondrial MitoTracker green probe to confirm the internalization of AMVs by PCCs in vitro (Figure 2A and 2C). After 2 hours of incubation, the DCPy (red) of AMVs had the most mitochondrial accumulation compared to other control groups. As shown in Figure S11, DCPy could be quickly released from AMVs under US radiation, which showed that ROS produced by DCPy could destroy AMVs structure. Subsequently, we verified the targeting ability of AMVs and ALVs to T24 cells and found that ALVs had the best mitochondrial targeting ability

to T24 cells (Figure S12). The CLSM images showed significant binding when the donor vesicles matched with their host cells and weak binding in cases of mismatch. This confirmed that the homologous targeting ability of AMVs was inherited from their parent PCCs. Recently, it has been studied that the homologous targeting ability associated with tumor cell membrane is mediated by integrin αvβ3 on the cell membrane surface.[29] It should be noted that although ALVs and PCCs have different sources, ALVs still have better tumor targeting ability against PCCs compared with APs, which may be caused by the cross-reaction activity between ALVs and PCCs.[30] Fluorescence lifetime imaging microscopy (FLIM) has been used to determine the extracellular vesicles that enter the cell by membrane fusion or by endocytosis.[31] A large mitochondrial membrane potential (approximately 180 mV) drives the capability of the cationic lipophilic DCPy to target the mitochondria, thus, providing a theoretical basis for the tumor-targeting potential of the AMVs.[32]

AMVs showed good biocompatibility with normal cells and did not inhibit cell growth at high concentrations (Figure S13). Optimum SDT requires efficient ROS generation by DCPy and AMVs. Thus, we assessed the SDT efficacy of AMVs. We used 2,7-Dichlorodihydrofluorescein diacetate (DCF) to measure ROS levels, which showed strong green fluorescence post US irradiation for both PCCs and AMVs (Figure 2B and 2D). However, the green fluorescence of the ALVs and APs groups was much weaker. This is due to the good homologous targeting ability of AMVs and the efficient ROS production efficiency of DCPy. Treatment with AMVs resulted in considerable toxicity post US irradiation, which reduced the cell viability to 6.5% in response to a 12 μg/mL DCPy (Figure S15). The growth inhibition rate of tumor cells in AMVs group was considerably greater compared with the other control groups. Tumor cell survival was assessed using fluorescein diacetate (FDA) single staining as DCPy fluorescence interfered with PI staining (Figure S16). The results were in agreement with the results of the MTT assay. The above experimental results showed that AMVs can effectively perform SDT on PCCs.

We next investigated the mechanism of the inhibition of cell survival by AMVs under US (Figure S14). Western blot analysis showed that the treatment of PCCs with AMVs could increase the protein expression of Bax, and markedly decrease the level of Bcl-2, which results in the enhancement of Bax/Bcl-2 ratio (Figure S14A and S14B). Besides, more Cytochrome c (Cyt c) also can be delivered from mitochondria to cytosol. Caspase-3 also undergoes a more prominent increase of cleaved caspase-3 (Figure S14C). The above data demonstrated that AMVs can cause apoptosis through the mitochondrial dependent pathway under US.

An ideal anti-tumor technique should have favorable pharmacokinetics and systemic bio-distribution profiles apart from high cytotoxicity and rapid internalization by PCCs.[33] Next, we evaluated the biodistribution of the APs, AMVs, and ALVs in PDX-bearing mice (n=3). Twelve hours post-injection, mice were euthanized, followed by isolation of tumors and major organs, which were imaged using an IVIS small animal imaging system with Cy5 channel (Figure 3A). APs were rapidly eliminated from the blood circulation compared with AMVs and ALVs, which showed increased blood retention of AMVs and ALVs (Figure 3B). The in vitro imaging data of mouse organs can directly illustrate the distribution of DCPy in vivo. DCPy fluorescence distribution profile in the tumors was measured by ZEN software (Figure 3C). While it can be observed that AMVs exhibited more effective tumor tropism in PDX bearing mice than ALVs and APs. The results of ex vivo imaging demonstrated that AMVs targeted homotypic PDX efficiently. Quantitative analysis showed that the fluorescence intensities in the tumor area of mice injected with AMVs and ALVs were 1.66 and 2.38 times

higher than that of APs at 12 h post-injection, respectively (Figure 3D). We also studied the fluorescence intensity of tumor tissues at various time points after administration, and found that AMVs had the best tumor targeting at different time points (Figure 3E). The tumor membrane proteins derived AMV are known to regulate their internalization in the target tissues. Recent studies have indicated the possibility of cargo permeability through these proteins.[18, 22] However, further research focusing on the mechanism of this unique homotypic tumor-targeting effect is required. In general, our experimental results showed that AMVs has personalized tumor targeting ability and can efficiently deliver DCPy to PDX tumor tissue, which provides experimental basis for subsequent personalized SDT.

Motivated by the above proof in vivo, the therapeutic effect was further assessed on the PDX-bearing mice. Intratumoral ROS levels were determined using DCF in PDX-bearing mice after different treatments. The results showed considerably DCF staining in tumors of the AMVs-treated mice post US treatment (Figure 4A and 4B). Cells in the ALVs with US group showed relatively weak fluorescence. We used mice having PDX tumors to further investigate the anti-tumor efficacy of the AMVs. These animals were randomly divided into six treatment groups: (1) PBS; (2) US; (3) AMVs; (4) APs+US; (5) ALVs+US; and (6) AMVs+US. The DCPy dose was 5mg/kg in groups 3, 4, 5, and 6. The SDT (power density = 0.75 W/cm^2, transducer frequency = 1 MHz, 30% duty cycle, 10 min) was performed 12 h after intravenous injection. The results demonstrated increased tumor growth in the control group. As shown in Figure 4C, the tumors grew rapidly in the control group to a maximum of 594 mm^3. Partial tumor growth inhibition was observed on treatment with the combination of ALVs and US irradiation whereas US or AMVs alone posed a slightly damage to the tumor tissue, which indicated that the single US or non-homotypic AMVs could not realize an admirable therapeutic effect. Significantly, treatment with AMVs and US irradiation showed maximum growth inhibition and no recurrent growth was observed. Thus, AMVs-mediated homotypic targeting of the PDX tumors sufficiently improved the effectiveness of SDT. We observed no substantial treatment-induced alterations in body weight over the study period (Figure 4D), which indicated minimal systemic toxicity. Additionally, hematoxylin and eosin (H&E) staining revealed that combined treatment with AMVs and US induced a significant tumor tissue loss consistent with extensive necrosis or apoptosis (Figure 4E). Furthermore, the mean tumor size and weight of all groups shown in Figure 4F and 4G, the results also demonstrated that the combination of excellent tumor-targeted AMVs and enhanced US owned the greatest inhibitory tumor effect. Next, we evaluated the overall histological specimens of H&E-stained lung, liver, heart, spleen, and kidney sections from these animals to confirm the absence of AMVs-induced systemic toxicity. The results confirmed the absence of major anomalies in any mice (Figure S17). Also, liver or kidney function were not impaired (Figure S18). Thus, AMVs treatment did not result in any serious adverse events in this murine. In general, the AMVs system constructed by us can effectively perform SDT in PDX models, which is the first study to verify the efficacy of AIEgens on the PDX model, and provides a good reference for the clinical application of AIEgen in the future.

.

Conclusions

In summary, we have designed a patient-derived MVs/AIEgen hybrid system for personalized SDT in bladder cancer patient-derived xenograft models. We first collected tumor tissues from patient bearing bladder tumors to develop PDX cell/mouse models. Meanwhile, we separated the PCCs from patient tumor tissues, and they were then prepared into PCVs. Subsequently,

the electroporation method was used to prepare AMVs. We extended the research of AIEgen in SDT and found that DCPy can simultaneously produce two kinds of reactive oxygen species. We combined PCVs with DCPy for personalized sonodynamic therapy of PDX tumors. The AMVs system we constructed has a good homologous tumor-targeting ability. Compared with APs or non-homologous vesicles system (ALVs), AMVs had the best sonodynamic therapeutic effect in PDX models. It is worth noting that the combination of AMVs and US can effectively kill cancer cells and significantly inhibit tumor growth. Our research provides a reliable theoretical basis and experimental data for the clinical application of AIEgens. It also provides new ideas for the design of the SDT system and AIEgens. In the future, we will develop new AIEgens with higher ROS production rate under US radiation and focus on solving the problem of hypoxia tolerance in the treatment of sonodynamic therapy. We will also combine the SDT and tumor immunotherapy to carry out research. We will further promote the research of AIEgens in the SDT and promote the clinical application of AIEgens.

Experimental Section

The detail experimental processes are available in the Supporting Information.

Acknowledgements

D. Z. and Z. Z. contributed equally to this work. We are grateful for the financial support from the State Key Research Development Program of China (Grant No. 2019YFB2203503), National Natural Science Foundation of China (Grant No. 61875138, 61435010, and 61961136001), the Research Grants of Council of Hong Kong (N-HKUST609/19, A-HKUST605/16 and C6009-17G) and the Innovation of Technology Commission (ITC-CNERC14SC01). The author would like to thank Dr. Fei Huang from Shiyanjia Lab (www.shiyanjia.com) for drawing schematic diagram and Dr. Yuanqiao He for establishment of PDX models.

Conflict of Interest

The authors declare no conflict of interest.

Received: ((will be filled in by the editorial staff))
Revised: ((will be filled in by the editorial staff))
Published online: ((will be filled in by the editorial staff))

References

[1] Y. Chen, J. W. Y. Lam, R. T. K. Kwok, B. Liu, B. Z. Tang, Materials Horizons 2019, 6, 428; J. Li, J. Wang, H. Li, N. Song, D. Wang, B. Z. Tang, Chemical Society reviews 2020, 49, 1144.

[2] S. Wang, J. Liu, C. C. Goh, L. G. Ng, B. Liu, Advanced materials 2019, 31, e1904447; S. Liu, C. Chen, Y. Li, H. Zhang, J. Liu, R. Wang, S. T. H. Wong, J. W. Y. Lam, D. Ding, B. Z. Tang, Advanced Functional Materials 2019, 30, 1908125; X. Shi, C. Y. Y. Yu, H. Su, R. T. K. Kwok, M. Jiang, Z. He, J. W. Y. Lam, B. Z. Tang, Chemical science 2017, 8, 7014; Kenry, Y. Duan, B. Liu, Advanced materials 2018, 30, e1802394; X. Ni, X. Zhang, X. Duan, H.-L. Zheng, X.-S. Xue, D. Ding, Nano letters 2019, 19, 318; X. Guo, B. Cao, C. Wang, S. Lu, X. Hu, Nanoscale 2020, 12, 7651.

[3] C. Y. Yu, H. Xu, S. Ji, R. T. Kwok, J. W. Lam, X. Li, S. Krishnan, D. Ding, B. Z. Tang,

Advanced materials 2017, 29.
[4] Z. Zheng, T. Zhang, H. Liu, Y. Chen, R. T. K. Kwok, C. Ma, P. Zhang, H. H. Y. Sung, I. D. Williams, J. W. Y. Lam, K. S. Wong, B. Z. Tang, ACS nano 2018, 12, 8145.
[5] F. Gao, J. Wu, H. Gao, X. Hu, L. Liu, A. C. Midgley, Q. Liu, Z. Sun, Y. Liu, D. Ding, Y. Wang, D. Kong, X. Huang, Biomaterials 2020, 230, 119635; G. Feng, B. Liu, Small 2016, 12, 6528.
[6] D. Zhu, Y. Duo, S. Meng, Y. Zhao, L. Xia, Y. Li, B. Z. Tang, Angewandte Chemie 2020, 59, 2-10.
[7] F. Hu, S. Xu, B. Liu, Advanced materials 2018, 30, 1801350; L. Zhang, Y. Li, W. Che, D. Zhu, G. Li, Z. Xie, N. Song, S. Liu, B. Z. Tang, X. Liu, Z. Su, M. R. Bryce, Advanced science 2019, 6, 1802050; C. Zhu, R. T. K. Kwok, J. W. Y. Lam, B. Z. Tang, ACS Applied Bio Materials 2018, 1, 1768; C. Chen, X. Ni, S. Jia, Y. Liang, X. Wu, D. Kong, D. Ding, Advanced materials 2019, 31, 1904914.
[8] X. Qian, Y. Zheng, Y. Chen, Advanced materials 2016, 28, 8097; J. Moan, K. Berg, Photochemistry and Photobiology 1991, 53, 549.
[9] P. Zhu, Y. Chen, J. Shi, ACS nano 2018, 12, 3780.
[10] X. Pan, L. Bai, H. Wang, Q. Wu, H. Wang, S. Liu, B. Xu, X. Shi, H. Liu, Advanced materials 2018, 30, e1800180; S. Son, J. H. Kim, X. Wang, C. Zhang, S. A. Yoon, J. Shin, A. Sharma, M. H. Lee, L. Cheng, J. Wu, J. S. Kim, Chemical Society reviews 2020.
[11] Z. Gao, J. Zheng, B. Yang, Z. Wang, H. Fan, Y. Lv, H. Li, L. Jia, W. Cao, Cancer letters 2013, 335, 93; N. Miyoshi, T. Igarashi, P. Riesz, Ultrasonics Sonochemistry 2000, 7, 121; S. Umemura, K. Kawabata, K. Sasaki, N. Yumita, K. Umemura, R. Nishigaki, Ultrasonics Sonochemistry 1996, 3, S187.
[12] J. Chen, H. Luo, Y. Liu, W. Zhang, H. Li, T. Luo, K. Zhang, Y. Zhao, J. Liu, ACS nano 2017, 11, 12849.
[13] K. M. Buettner, A. M. Valentine, Chemical reviews 2012, 112, 1863.
[14] V. G. Deepagan, D. G. You, W. Um, H. Ko, S. Kwon, K. Y. Choi, G.-R. Yi, J. Y. Lee, D. S. Lee, K. Kim, I. C. Kwon, J. H. Park, Nano letters 2016, 16, 6257.
[15] Y. Li, Q. Wu, M. Kang, N. Song, D. Wang, B. Z. Tang, Biomaterials 2020, 232, 119749.
[16] L. Shi, F. Hu, Y. Duan, W. Wu, J. Dong, X. Meng, X. Zhu, B. Liu, ACS nano 2020; H.-T. Feng, J. W. Y. Lam, B. Z. Tang, Coordination Chemistry Reviews 2020, 406, 213142.
[17] T. Yong, D. Wang, X. Li, Y. Yan, J. Hu, L. Gan, X. Yang, Journal of controlled release : official journal of the Controlled Release Society 2020; S. Walker, S. Busatto, A. Pham, M. Tian, A. Suh, K. Carson, A. Quintero, M. Lafrence, H. Malik, M. X. Santana, J. Wolfram, Theranostics 2019, 9, 8001; J. Lee, J. Kim, M. Jeong, H. Lee, U. Goh, H. Kim, B. Kim, J. H. Park, Nano letters 2015, 15, 2938.
[18] D. Wang, Y. Yao, J. He, X. Zhong, B. Li, S. Rao, H. Yu, S. He, X. Feng, T. Xu, B. Yang, T. Yong, L. Gan, J. Hu, X. Yang, Advanced science 2019, 1901293.
[19] K. Tang, Y. Zhang, H. Zhang, P. Xu, J. Liu, J. Ma, M. Lv, D. Li, F. Katirai, G.-X. Shen, G. Zhang, Z.-H. Feng, D. Ye, B. Huang, Nature communications 2012, 3.
[20] X. Dong, J. Gao, C. Y. Zhang, C. Hayworth, M. Frank, Z. Wang, ACS nano 2019, 13, 1272; D. Yang, W. Zhang, H. Zhang, F. Zhang, L. Chen, L. Ma, L. M. Larcher, S. Chen, N. Liu, Q. Zhao, P. H. L. Tran, C. Chen, R. N. Veedu, T. Wang, Theranostics 2020, 10, 3684.
[21] G. Fuhrmann, A. Serio, M. Mazo, R. Nair, M. M. Stevens, Journal of controlled release : official journal of the Controlled Release Society 2015, 205, 35; W. Zhang, Z. L. Yu, M. Wu, J. G. Ren, H. F. Xia, G. L. Sa, J. Y. Zhu, D. W. Pang, Y. F. Zhao, G. Chen, ACS nano 2017, 11,

277.
[22] Q. Liang, N. Bie, T. Yong, K. Tang, X. Shi, Z. Wei, H. Jia, X. Zhang, H. Zhao, W. Huang, L. Gan, B. Huang, X. Yang, Nature biomedical engineering 2019, 3, 729.
[23] X. Huang, G. Deng, Y. Han, G. Yang, R. Zou, Z. Zhang, S. Sun, J. Hu, Advanced science 2019, 6, 1901461; S. Liu, H. Li, L. Xia, P. Xu, Y. Ding, D. Huo, Y. Hu, Biomaterials 2017, 141, 1.
[24] S. K. Golombek, J.-N. May, B. Theek, L. Appold, N. Drude, F. Kiessling, T. Lammers, Advanced drug delivery reviews 2018, 130, 17; Q. Sun, Z. Zhou, N. Qiu, Y. Shen, Advanced materials 2017, 29, 1606628.
[25] M. L. Schulte, A. Fu, P. Zhao, J. Li, L. Geng, S. T. Smith, J. Kondo, R. J. Coffey, M. O. Johnson, J. C. Rathmell, J. T. Sharick, M. C. Skala, J. A. Smith, J. Berlin, M. K. Washington, M. L. Nickels, H. C. Manning, Nature medicine 2018, 24, 194.
[26] Q. Chen, L. Xu, C. Liang, C. Wang, R. Peng, Z. Liu, Nature communications 2016, 7, 13193.
[27] X. Cai, D. Mao, C. Wang, D. Kong, X. Cheng., B. Liu., Angewandte Chemie 2018, 57, 16396.
[28] V. Misik, P. Riesz, in *Reactive Oxygen Species: From Radiation To Molecular Biology: A Festschrift In Honor Of Daniel L Gilbert*, Vol. 899 (Ed: C. C. Chiueh), New York Acad Sciences, New York 2000, 335.
[29] X. Xie, X. Hu, Q. Li, M. Yin, H. Song, J. Hu, L. Wang, C. Fan, N. Chen, Nano letters 2020.
[30] T. Yong, X. Zhang, N. Bie, H. Zhang, X. Zhang, F. Li, A. Hakeem, J. Hu, L. Gan, H. A. Santos, X. Yang, Nature communications 2019, 10, 3838.
[31] H. Saari, E. Lisitsyna, K. Rautaniemi, T. Rojalin, L. Niemi, O. Nivaro, T. Laaksonen, M. Yliperttula, E. Vuorimaa-Laukkanen, Journal of controlled release : official journal of the Controlled Release Society 2018, 284, 133.
[32] D. Zhu, Y. Duo, M. Suo, Y. Zhao, L. Xia, Z. Zheng, Y. Li, B. Z. Tang, Angewandte Chemie 2020.
[33] W. Xie, W. W. Deng, M. Zan, L. Rao, G. T. Yu, D. M. Zhu, W. T. Wu, B. Chen, L. W. Ji, L. Chen, K. Liu, S. S. Guo, H. M. Huang, W. F. Zhang, X. Zhao, Y. Yuan, W. Dong, Z. J. Sun, W. Liu, ACS nano 2019, 13, 2849; F. Gao, Y. Tang, W. L. Liu, M. Z. Zou, C. Huang, C. J. Liu, X. Z. Zhang, Advanced materials 2019, e1904639.

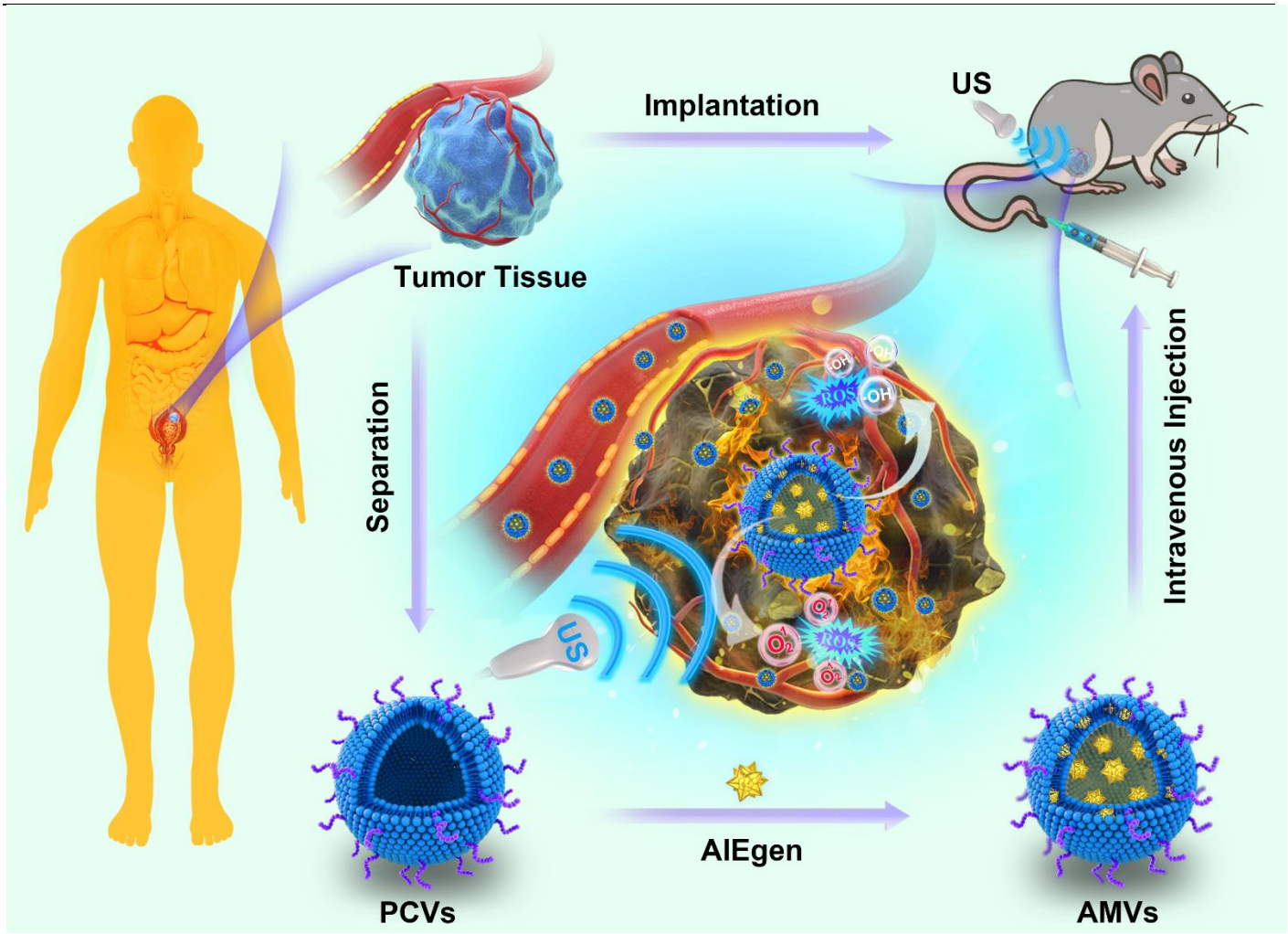

Scheme 1. The patient-derived microvesicles/AIE Luminogen hybrid system for personalized sonodynamic cancer treatment in patient-derived xenograft (PDX) models.

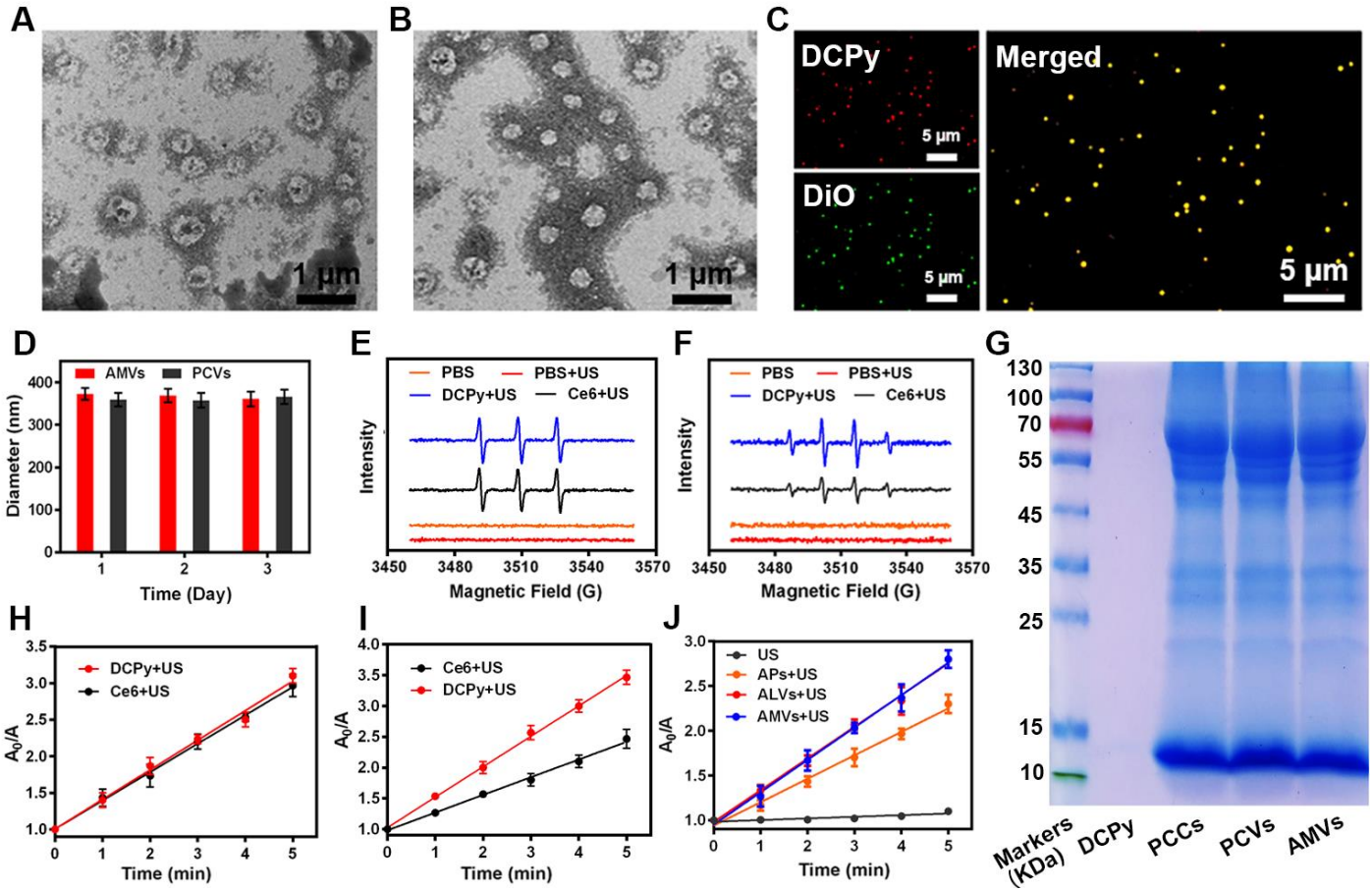

Figure 1. (A) TEM images of PCVs and (B) AMVs. (C) Confocal microscopic analysis of the colocalization of DCPy (red) and DiO (green) within the AMVs. (D) Assessment of the hydrodynamic diameter of AMVs and PCVs (in PBS) on days 1, 2, and 3 using DLS. Data were presented as mean ± SD. (E) $^1O_2$ generation by PBS, DCPy, and Ce6 with/without ultrasound (US) radiation using ESR. (F) •OH generation by PBS, DCPy, and Ce6 with/without US using ESR. (G) SDS-PAGE protein patterns of PCCs, PCVs, AMVs, and DCPy. (H) Decomposition rates of ABDA induced by $^1O_2$ generation for DCPy or Ce6 under US radiation. (I) Decomposition rates of MB induced by •OH generation for DCPy or Ce6 under US radiation. (J) Decomposition rates of ABDA induced by ROS generation from different formulations under US (1.0 MHz, 0.75 W/cm^2, 5 min).

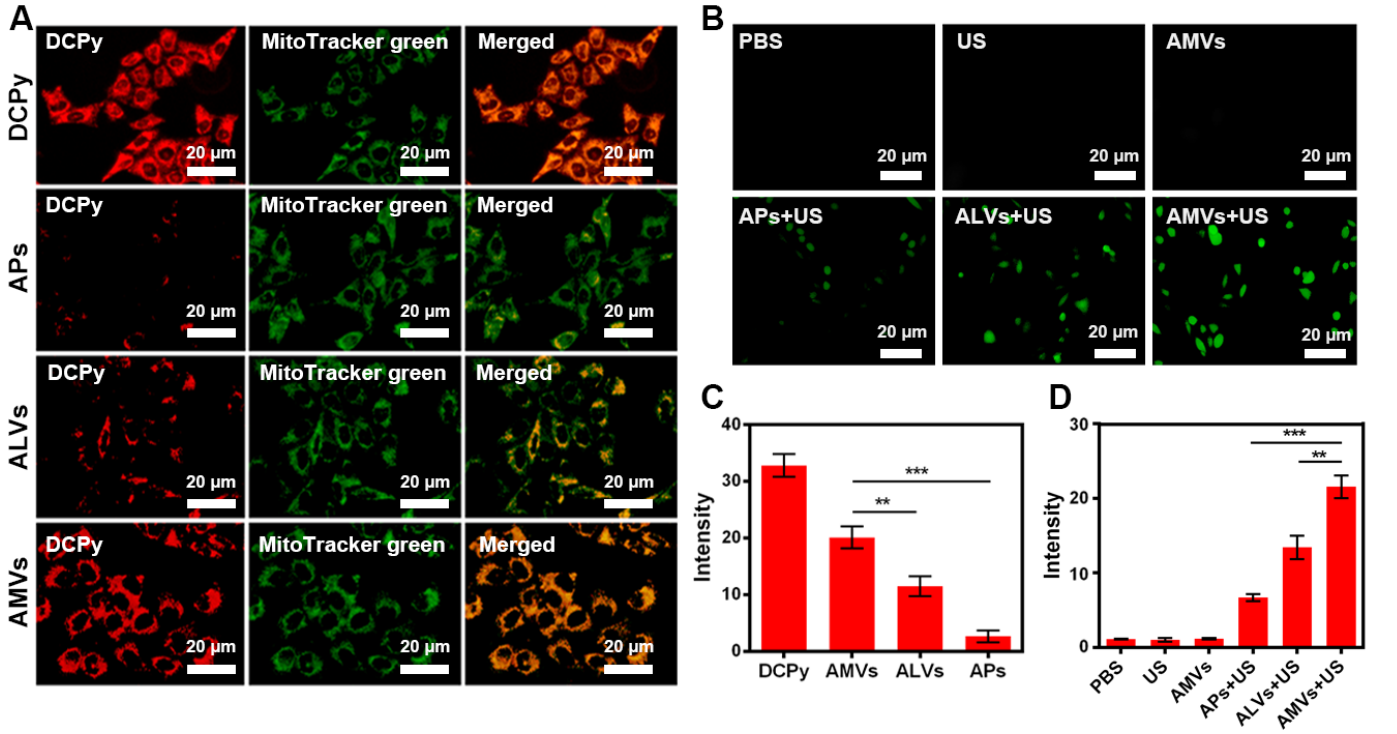

Figure 2. (A) Colocalization of DCPy (red) and Mito-tracker green (green) for APs, ALVs, and AMVs over time in patient derived cancer cells (PCCs). (B) CLSM images of ROS generation in PCCs after different treatments. (C) Quantification of DCPy fluorescence intensity in A was done using ImageJ. Data were expressed as mean ± SD. *P < 0.01, **P < 0.005, ***P < 0.001; Student's t-test. (D) Quantification of 2, 7-Dichlorodihydrofluorescein diacetate (DCF) fluorescence intensity in B was done using ImageJ. Data were presented as mean ± SD. *p < 0.01, **p < 0.005, ***p < 0.001; Student's t-test.

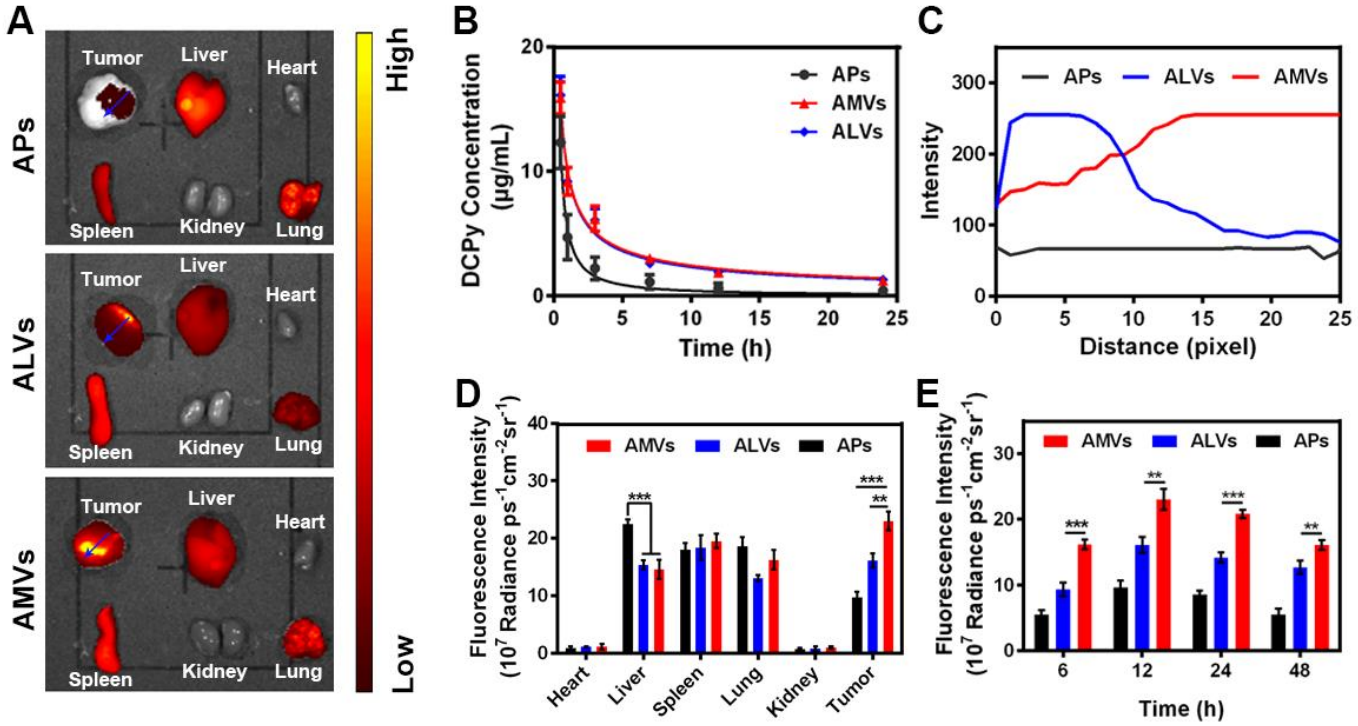

Figure 3. (A) Ex vivo images of excised organs and tumors of mice bearing PDX examined at 12 h post-injection of APs, ALVs, and AMVs in the presence of DCPy (5 mg/kg). (B) The pharmacokinetic behaviors of APs, AMVs, and ALVs in mice after intravenous injection at

DCPy (5 mg/kg). Data were expressed as mean ± SD. (C) DCPy fluorescence distribution profile on the specified blue arrows in tumors of Figure 3A. (D) Quantification of DCPy fluorescence intensity 12 h post-injection of APs, ALVs, and AMVs in the presence of DCPy (5 mg/kg). Data were presented as mean ± SD. *p < 0.01, **p < 0.005, ***p < 0.001; Student's t-test. (E) Quantification of the time-dependent fluorescence intensity at the tumor site after injection of APs, ALVs, and AMVs at a DCPy equivalent dose of 5 mg/kg. Data were expressed as mean ± SD. *p < 0.01, **p < 0.005, ***p < 0.001; Student's t-test.

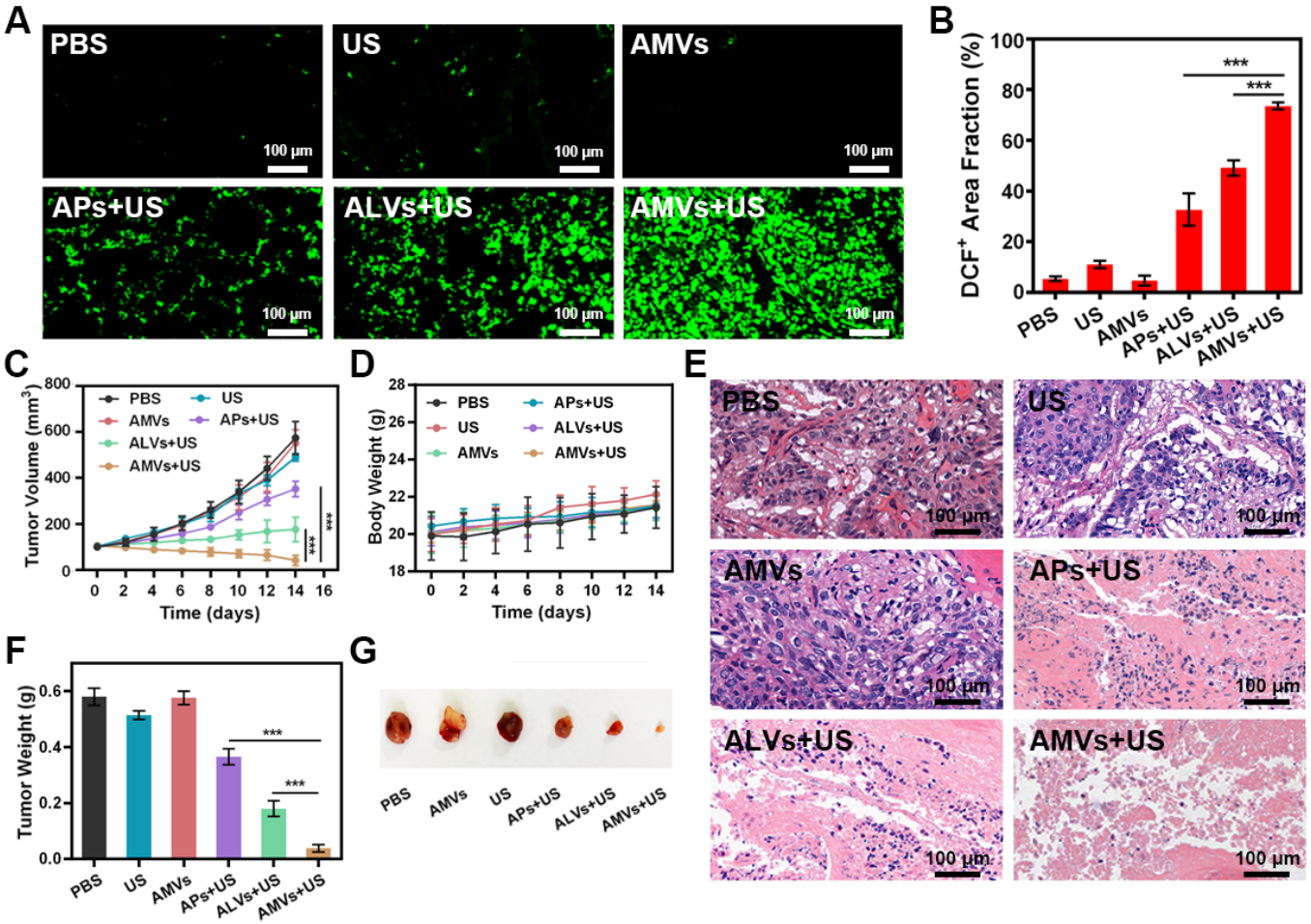

Figure 4. (A) Measurement of ROS levels in DCF-stained tumor sections after different treatment. (B) Quantification of area fraction of DCF fluorescence from Figure 4A. Data were expressed as mean ± SD. *P < 0.01, **P < 0.005, ***P < 0.001; Student's t-test. (C) Tumor volume and (D) body weight curves after the treatment in the bladder cancer PDX model. Data were expressed as mean ± SD. *P < 0.01, **P < 0.005, ***P < 0.001; Student's t-test. (E) Representative H&E staining images of tumor slices in the mice after different treatments. (F) Tumor weight and (G) tumor tissues collected from the PDX mice after various treatments. Data were presented as mean ± SD. *P < 0.01, **P < 0.005, ***P < 0.001; Student's t-test

The Table of Contents Entry

A patient-derived MVs/AIEgen hybrid system (AMVs) was developed in this work for personalized SDT in bladder cancer patient-derived xenograft (PDX) models. Impressively, AMVs displayed better tumor targeting ability and personalized SDT therapy compared with PLGA/AIEgen hybrid nanoparticles and cell line-derived micro vesicles. This work presented the first example of AIEgen-based hybrid system as sonosensitizer for SDT and PDX tumors therapy.

Keywords: Aggregation-Induced Emission, Sonosensitizers, Personalized Sonodynamic Cancer Therapy, Patient-Derived Microvesicles, Patient-Derived Xenograft Models

Daoming Zhu, Zheng Zheng, Meng Suo, Zeming Liu, Yanhong Duo* and Ben Zhong Tang*

Patient-Derived Microvesicles/AIE Luminogen Hybrid System for Personalized Sonodynamic Cancer Therapy in Patient-Derived Xenograft Models